Ref. Ares(2026)5457287 - 29/05/2026

OPINCHARGE

PROJECT
D2.2 - Assessment/quantification of side-reaction intensity - Identification of compositions (electrode/electrolyte) promoting passivation / the oxidative dissolution of cathode materials

Month 36 (May 31st / 2026)

Funded by the European Union

Lead Beneficiary	CNRS- France
Author(s)/Organisation(s)	I.T. LUCAS - CNRS
Contact Email	Ivan.lucas@CNRS-IMN.fr
Contributor(s)	I.T. LUCAS, R. HANIFAH
Work Package	2 – Task 2.1 & 2.2
Delivery Date (DoA)	M36 – 31st of May 2026
Actual Delivery Date	**29.05.2026**
Abstract:	This report covers two axes within the same deliverable dedicated to side reactions: **(i)** the dynamics of SEI formation and composition by operando SHINERS and **(ii)** the metal dissolution from positive electrodes and subsequent cross-contamination within the cell using electrochemical sensing. The two sections are preceded by a summary of the highlights.

Document Revision History			
Date	**Version**	**Author/Contributor/Reviewer**	**Summary of Main Changes**
28/05/2026	V1	LUCAS Ivan, HANIFAH Rizki	

Dissemination Level and Nature of the Deliverable		
PU	Public	
SEN	Sensitive, limited under the conditions of the Grant Agreement	x
Nature	R = Report, E = Ethics or, O = Other	R

Funded by the European Union

OPINCHARGE Consortium			
#	Participant Organisation Name	Short Name	Country
1	LUXEMBOURG INSTITUTE OF SCIENCE AND TECHNOLOGY (LIST)	LIST	LU
2	CENTRE NATIONAL DE LA RECHERCHE SCIENTIFIQUE CNRS (CNRS)	CNRS	FR
3	CENTRO DE INVESTIGACION COOPERATIVA DE ENERGIAS ALTERNATIVAS FUNDACION, CIC ENERGIGUNE FUNDAZIOA (CIC ENERGIGUNE)	CIC ENERGIGUNE	ES
4	DEUTSCHES ZENTRUM FUR LUFT - UND RAUMFAHRT EV (DLR)	DLR	DE
5	DEUTSCHES FORSCHUNGSZENTRUM FUR KUNSTLICHE INTELLIGENZ GMBH (DFKI)	DFKI	DE
6	FEI ELECTRON OPTICS BV (THERMO)	THERMO	NL
7	FUNDACION CIDETEC (CIDETEC)	CIDETEC	ES
8	FORSCHUNGSZENTRUM JüLICH (FZJ)	FZJ	DE
9	PEDAL CONSULTING SRO (PEDAL)	PEDAL	SK
10	PAUL SCHERRER INSTITUT (PSI)	PSI	CH

NOTICE

Funded by the European Union under grant agreement number 101104032 . Views and opinions expressed are however those of the author(s) only and do not necessarily reflect those of the European Union or European Climate, Infrastructure and Environment Executive Agency (CINEA). Neither the European Union nor the granting authority can be held responsible for them.

OPINCHARGE

Grant Agreement: 101104032 .

Call: HORIZON-CL5-2022-D2-01.

Topic: HORIZON-CL5-2022-D2-01-02.

Type of action: HORIZON Research and Innovation Actions.

Granting authority: European Climate, Infrastructure and Environment Executive Agency.

Grant managed through EU Funding & Tenders Portal: Yes (eGrants).

Project starting date: fixed date: 1 June 2023.

Project end date: 31 May 2026.

Project duration: 36 months.

Copyright notice: © OPINCHARGE Consortium, 2023 - 2026.

Reproduction is authorised provided the source is acknowledged.

Funded by
the European Union

Table of Contents

1 Assessment/quantification of side-reaction intensity - Identification of compositions (electrode/electrolyte) promoting passivation 6

1.1 Approach and implementation 6

1.2 Interfacial compositions on copper electrodes for anode-less batteries 7

1.2.1 Dynamic of interfacial composition on Cu-Li electrodes by SHINERS 7

1.2.2 Impact of the electrolyte composition 9

1.3 Interfacial compositions on silicon anodes for LIBs 10

1.3.1 Dynamics of interfacial composition on Si-H thin films 10

1.3.2 Impact of the electrolyte composition 11

2. Assessment/quantification of side-reaction intensity - Identification of compositions (electrode/electrolyte) promoting the oxidative dissolution of cathode materials 13

2.1 Approach and implementation 14

2.2 Operando crosstalk sensing on battery materials 15

2.2.1 LNMO positive electrode materials (half-cell vs full-cell) 15

2.2.2 Other positive electrode materials 18

List of Figures

Figure 1: **NIR SHINERS** 7
Figure 3: Operando SHINERS on Cu-Li (charge) 8
Figure 4: Operando SHINERS on Cu-Li (discharge) 9
Figure 5: Operando SHINERS on Cu-Li (charge) in various electrolyte compositions 10
Figure 6 : **Operando SHINERS on doped Si (1st charge/discharge)** 11
Figure 7: Operando SHINERS on doped Si (1st charge/discharge) in various electrolyte composition 12
Figure 8: **Band intensity buildup at the end of the successive discharges of doped Si** 13
Figure 9 Crosstalk sensing device 14
Figure 10: Crosstalk sensing on the operating LNMO/Li system & impact of the electrolyte composition 16
Figure 11: Electrochemical signature of redox shuttles 17
Figure 12: Selective crosstalk quantification 17
Figure 13: Crosstalk sensing on full cell (LNMO/graphite). 18
Figure 14: Crosstalk sensing on the operating NMC811/Li system. 18

Funded by the European Union

This report covers two axes within the same deliverable dedicated to side reactions: **(i)** the dynamics of SEI formation and composition by operando SHINERS and **(ii)** the metal dissolution from positive electrodes and subsequent cross-contamination within the cell using electrochemical sensing. The two sections are preceded by a summary of the highlights.

1 Assessment/quantification of side-reaction intensity - Identification of compositions (electrode/electrolyte) promoting passivation

Highlights	
Results	Dynamics of interfacial composition (SEI) captured by Near-IR enhanced Raman spectroscopy on copper & doped silicon substrates, not by standard Raman – No evidence of beam damage
	Evidence of spontaneous SEI formation upon contact with the electrolyte, then evolution of the composition upon cycling
	Radical SEI composition changes at low potential before and after Li-plating on Cu current collector – Contrasted SEI composition and Li plated structures between mixte carbonate electrolyte (EC/DEC, EC/EMC) and cyclic one (PC)
	Evidence of SEI formation and partial redissolution on doped-Si upon charging & discharging, more pronounced in LP40 as compared to LP57 and LP10 resulting in a thicker but more heterogeneous surface film on the electrode.
Outcomes	2 invited review papers: Energy Storage Materials 73, 103794, 2024 / ACS nano 18 (43), 29337-29379, 2024.
	Collaboration with SAFT (Total group) – Operando Raman and pH-SERS on aqueous Zn/MnO_2 batteries

1.1 Approach and implementation

Raman microscopy measurements with boosted sensitivity were applied successfully to **copper current collectors for anode-less batteries (Li metal batteries LMBs)** and also **silicon anodes for lithium ion batteries (LIBs)** to resolve interfacial composition (SEI) in various electrolyte compositions (**LP40**: EC/DEC $LiPF_6$, **LP57**: EC/EMC $LiPF_6$, **LP10**: PC $LiPF_6$ purchased from Solvionic).

Reliable SHINERS in LMBs and LIBs conditions - Our approach to operando sensing of the LIB interface proposes a more versatile declination of Surface Enhanced Raman Spectroscopy (SERS) using shell-isolated nanoparticles as Raman signal amplifiers (**SHIN**), which can be implemented on any materials (i.e. not only plasmonic electrodes such as gold). Our developments fully described in the final report and D2.1 (M24) focused on:

Funded by the European Union

- The design of spectro-cells that allow access to the interface within the battery assembly with Raman microscopy while maintaining performance: ***coin-cells modified to accommodate an optical window***
- The design of SHINs that can operate under LIB conditions (organic electrolyte, large potential window): ***large anisotropic Au@SiO₂ core-shell nanoparticles which resonate in the NIR***
- The design of SHINERS experiments ***that minimize beam damage to the LIB electrolyte: specific microRaman probe (laser beam) shape to better control the photon dose***

Implementation - To deconvolute the **enhanced interfacial signal from the bulk signal** (electrode and electrolyte), microRaman measurements implemented on sample decorated with SHINs (***"interfacial" + "bulk" signal***) were systematically confronted to measurements on the same sample without SHIN (***bulk signal only***) using the same Raman probe (785 nm). Colloidal SHINs were deposited on pristine electrodes (drop casting) prior to the battery cell assembly. Raman spectra were collected in the ***"line"*** mode (elongated laser beam shape, 1% of the nominal laser power:0.5mW, 4x8s acquisitions), on three different locations on the sample for each potential value explored upon charge and discharge of the Cu or Si electrode (3 CV cycling at 0.5 mVs^{-1}, all potential values are reported vs Li). Raman spectra were also collected after extended CV cycling (15 cycles) to assess the ageing of the SEI.

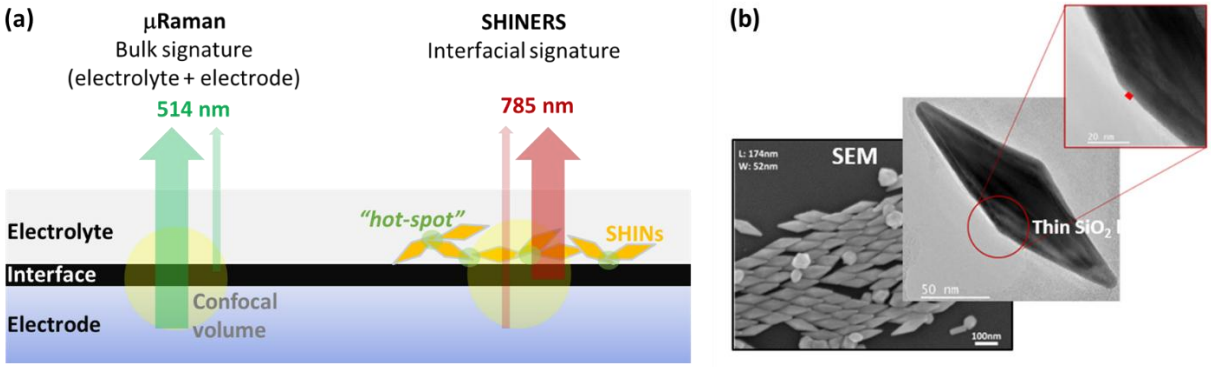

*Figure 1: **NIR SHINERS** - **(a)** Benefits of near-IR SHINERS for interfacial measurements as compared to conventional Raman probes (514 nm). The combined use of 785nm Raman excitation and large bipyramid SHINs allow strong interfacial signal enhancement while minimizing bulk contribution (electrode & electrolyte). **(b)** large anisotropic SHIN (Au@SiO_2 core-shell nanoparticles) deposited on the electrode surface.*

1.2 Interfacial compositions on copper electrodes for anode-less batteries

1.2.1 Dynamic of interfacial composition on *Cu-Li* electrodes by SHINERS

Copper foils (99.9% purity) were cleaned with ethanol in sonicated bath, rinse, decorated or not with SHINs, dried carefully and then assembled under inert atmosphere (0.1ppm) vs a lithium foil (half-cell) in modified coin-cells filled with 100µl electrolyte.

Charge/discharge without lithium plating/stripping (OCV – 0.01V) - **Surface copper oxide** was systematically detected at the OCV by SHINERS, not by standard microRaman (2 associated bands at 530 and 616cm^{-1} whose intensity decreases upon potential scan till full disappearance below 1V). The comparison of the SHINERS spectrum at the OCV with the µRaman one reveals extra bands associated to the **SEI spontaneously formed** upon contact of the copper electrode with the electrolyte. Then the increase of the current at the copper electrode for E<2V correlates with **changes of the interfacial**

Funded by the European Union
OPINCHARGE

composition: appearance of new mid-range bands 1375, 1395 cm^{-1} for E < 2V, 1281 & 1400 cm^{-1} for E < 0.5V which can be associated to organic carbonate type of compounds. For E<0.5V, a broad band at low wavenumber ≈500 cm^{-1} possibly associated to inorganic compounds (fluorinated compounds LiF, $LiPO_2F_2$, Li_2PO_3F, lithium hydroxide...). Upon discharge, very little changes are observed. The intensity of the broad bands at low wavenumbers (≈500 cm^{-1}) gradually decreases. The band at 1280 and 1843 that were still present at 0.1V, completely disappear at 1.5V.

Charge/discharge with lithium plating/stripping (OCV down to - 0.2V) – Upon lithium plating on copper, **a surge of signal** is observed, mainly at lower wave number (broad band typical of **inorganic compounds**) and also at high wave number where a sharp band characteristic of lithium acethylide (**Li_2C_2**) stands out[1]. At intermediate spectral range, the interfacial signature undergoes drastic modification, with new bands appearing: 804, 1060/1110, 1367, 1454, 1625 cm^{-1}. These changes are associated to the SEI formation on the freshly deposited lithium. The drastic increase of intensity, with bands now also visible in standard microRaman, can be explained by the strong accumulation of electrolyte degradation products (lithium deposits with high developed surface) and possibly also by an additional SERS effect provided by the nanostructured lithium deposit[2]. Note that the lithium deposition is associated with a radical change of optical contrast on micrograph images captured by the Raman optical microscope.

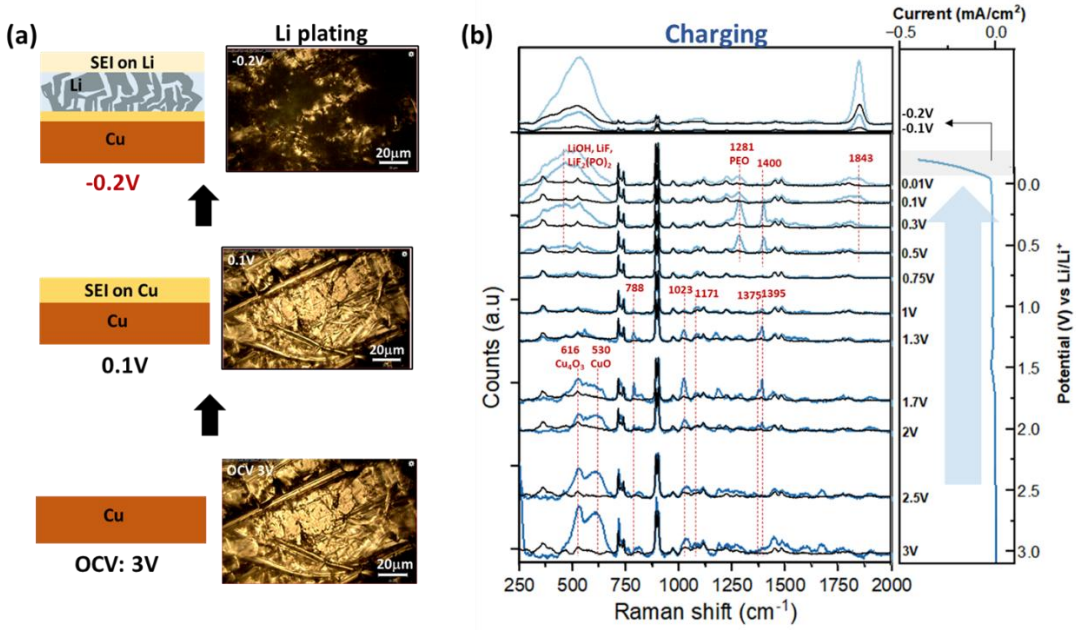

Figure 2: Operando SHINERS on Cu-Li (charge) - (a) *Optical microscopy image of pristine Cu at different polarization OCV, 0.1 (before Li plating), -0.2V (Cu with plated Li).* ***(b)*** *Dynamic of SEI formation on Cu upon charging to negative potential (-0.2V) using signal enhancement (SHINERS: colored spectra) or standard microRaman (no signal enhancement: black spectra)*

Upon lithium stripping, all band intensities decrease but remain much higher than that observed on copper when no lithium plating/stripping takes place. This implies that SEI products developed on Li persist at the interface even after Li stripping, or that the Li stripping is incomplete, as confirmed by optical micrograph (the bright contrast previously observed on bare copper is not recovered). The SEI dynamics on the plated lithium electrode during discharge are still clearly observed in the standard micro-Raman operando measurements, with lower intensity confirming the strong SEI accumulation and the additional SERS effect of the nanostructured lithium deposit[2].

Funded by the European Union
OPINCHARGE

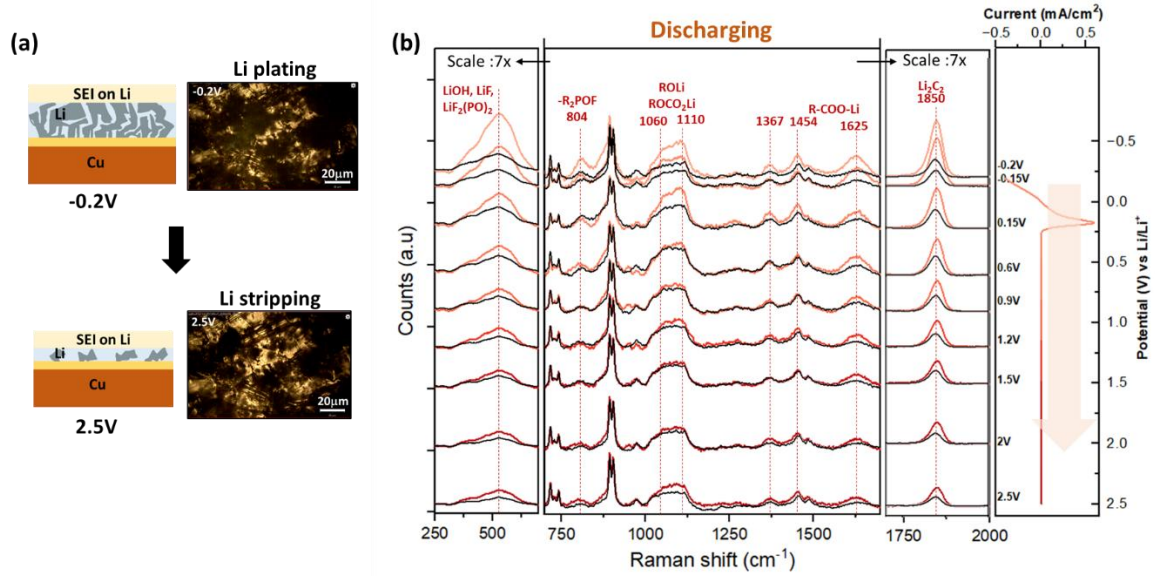

Figure 3: Operando SHINERS on Cu-Li (discharge) - (a) *Optical microscopy image of pristine Cu at different polarization, -0.2V (Cu with plated Li), and + 2.5V (Cu with Li incompletely stripped).* ***(b)*** *Dynamic of SEI formation on plated Li upon discharging using signal enhancement (SHINERS: colored spectra) or standard microRaman (no signal enhancement: black spectra).*

1.2.2 Impact of the electrolyte composition

Operando SHINERS experiments were repeated in LP57 and LP10 electrolytes:

- **At the OCV**, copper oxide and SEI layer (spontaneously formed) were observed for LP57, similarly to LP40 but with a lesser intensity. Note that spectra collected at the OCV in PC show a very strong background signal (fluorescence) which screened the Raman signal and saturates the detector. Interfacial signature could be recovered in PC during the potential scan after the fluorescence background drastically decreases (quenching) at 1.3V.
- **Upon charging**, all electrolytes exhibit similar interfacial chemistry and dynamics down to 0.5V, with similar bands appearing between 1000 & 1450 $cm^{-1,}$ with however a lower intensity in PC. Major differences appear at low potential before (0.01V) and upon plating (-0.2V), with a surge of signal associated to inorganic compounds at low wave number for LP40 and LP57 (broad band at 300-600 cm^{-1}) and at high wavenumber (1850 cm^{-1}: Li_2C_2), i.e. a 7-fold intensity difference with the band at mid wavenumber. SEI bands at low and high wavenumbers (300-600 cm^{-1} and 1850 cm^{-1}, respectively) in the LP10 electrolyte are much weaker than those observed in the LP40 and LP57 electrolytes. The vibrational signature around 1850cm^{-1}, quite different in PC corresponds to the overlapping of one PC electrolyte band and the band associated to lithium acetylide (Li_2C_2) or most likely methylacetylide ($CH_3C \equiv CLi$) for PC.

The strong variations in the band intensity at low and high wave number between binary and cyclic carbonate electrolytes correspond to different SEI composition and thicknesses/structures, i.e. a thick SEI dominated by inorganic compounds in LP40 and LP57. Different morphologies of the deposited lithium were observed on the copper current collector, finely branched dendrites in LP40 electrolyte, and coarser and coarser dendrites while moving from LP57 to LP10, underlying the intimate connection between the electrolyte composition, the SEI properties on Cu and Li and the subsequent lithium plating structure.

Funded by the European Union
OPINCHARGE

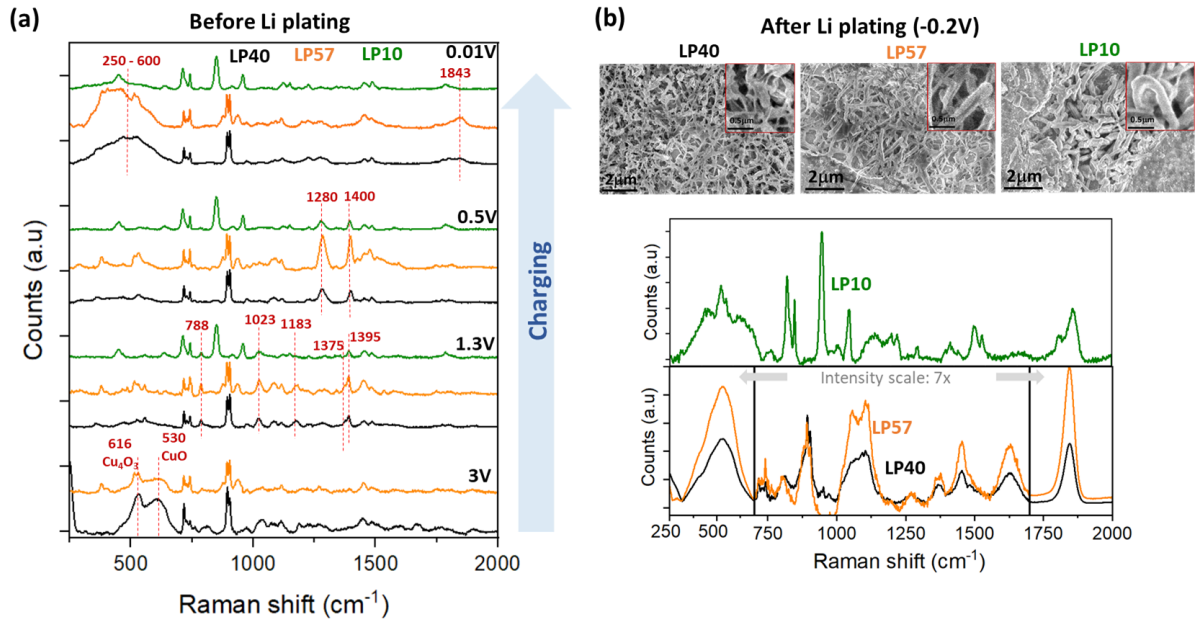

Figure 4: Operando SHINERS on Cu-Li (charge) in various electrolyte compositions *- (a) Dynamic of interfacial composition on Cu (1st charge) in three different electrolyte compositions (LP40, LP57, and LP10). (b) Different Li deposition morphology and SEI formation on plated Li depending on the electrolyte composition*

1.3 Interfacial compositions on silicon anodes for LIBs

Operando SHINERS has been applied to various silicon samples used as received or prepared by our partners: crystalline silicon (doped wafer ***c-Si***: 100), amorphous non-doped (***a-Si***) and doped (hydrogenated ***a-Si-H*** or methylated ***a-Si-Me***) silicon thin film (50nm thick) deposited on copper foil. Interfacial composition dynamics could be successfully extracted on doped ***Si-H*** and ***Si-Me*** samples only.

1.3.1 Dynamics of interfacial composition on Si-H thin films

Operando Raman measurement were conducted on ***Si-H vs Li*** in modified coin-cell (half-cell) filled with ***LP40 electrolyte*** *for the first 3 cycles*:

First charge **-** Clear interfacial responses were extracted on SHIN-decorated Si-H sample while without SHINs (bulk response of the electrolyte and of the electrode), no interfacial dynamics could be recovered, attesting of the necessity to amplify the signal of the interfacial compounds with low intrinsic Raman scattering cross section. Note that, the interfacial response at the OCV is different from the bulk response, meaning that the Si surface is already covered by compounds resulting for the **spontaneous decomposition of the electrolyte**. Additional Raman bands distinct from the one of electrolyte and of the electrode were also observed for ***c-Si*** and ***a-Si***, with however no intensity fluctuations upon polarization.

A strong increase intensity of various bands at higher Raman shifts (polycarbonate region: organic SEI) is observed starting from 0.75 V vs Li/Li^+, some of them being overlapped with the bands of the electrolyte (1074, 1141, 1266, 1450,1490 cm^{-1}). Note that the bands at 1074, 1141, 1266, 1450 cm^{-1} could match the one of lithium ethyl methyl carbonate LEMC[1], a possible SEI component resulting

[1] Comparison with reference Raman spectra obtained via calculation from our collaborator in Belgium or experimentally on LEMC synthesized in IMN.

Funded by the European Union

from the reduction of carbonate-based electrolytes. Changes were also observed at lower Raman shift (Li oxides and fluorides: inorganic SEI) but with lower intensity. Note that the early stage of formation of the SEI as high as 1.4 V, attested by the onset of reduction current on Si might not be fully detected by SHINERS, given that SEI accumulation remains low until 0.75 V. As accumulation increases at 0.5 V, a significant rise in band intensity is observed.

First discharge - Surprisingly, the intensity of the new bands observed during the first charge tends to progressively decrease upon delithiation. This specific behavior could originate from (i) a partial instability/dissolution of the SEI promoted by the large volume change of Si electrode upon delithiation, **(ii)** the accumulation/depletion of soluble species at the interface upon charging/discharging, **(iii**) the change in the optical properties of Si (increase of the metallic character) and of the resulting optical coupling with the superficial SHINs. As this apparent reversibility has been observed with SHINERS only on doped Si samples (Si-H and Si-Me) and even when no lithiation effectively takes place, **SEI formation/dissolution** can be incriminated. The built up of signal intensity cycle after cycle, implying only a partial dissolution and the progressive accumulation of decomposition products at the surface of the electrode tends to support also this hypothesis.

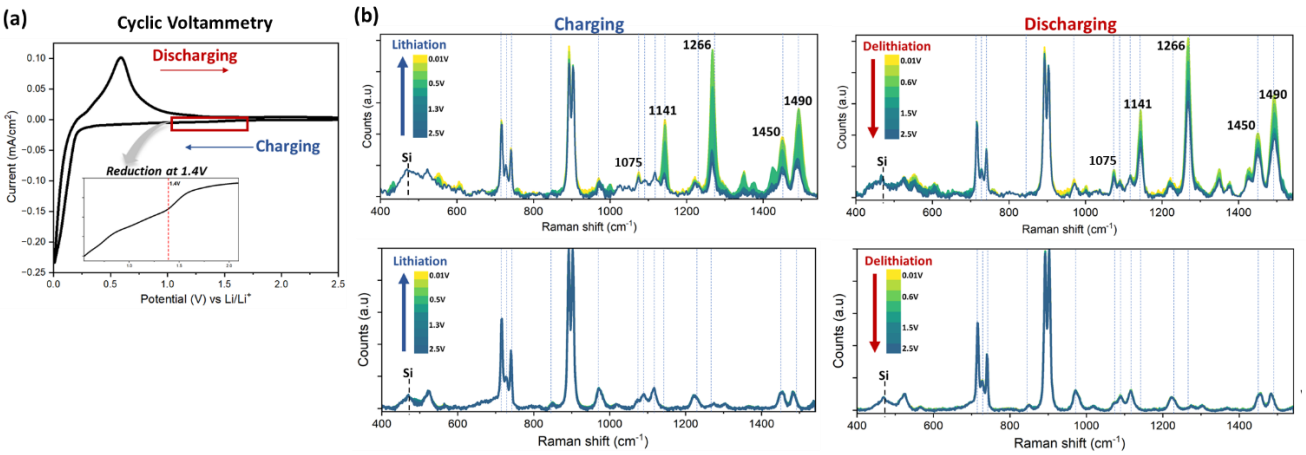

Figure 5 *: **Operando SHINERS on doped Si (1st charge/discharge) - (a)** CV cycling of the Si-H thin film in LP40 electrolyte. **(b)** Potential dependent Raman response upon charging and discharging - **Top**: with SHINS, **bottom:** without SHINERS (no potential dependent response)*

1.3.2 Impact of the electrolyte composition

Additional SHINERS operando data collected in LP57 and LP10 electrolytes evidenced a similar behavior: a Raman response at the OCV different from that of the electrolyte of the electrode, the increase of band intensity at low and high Raman shift and the partial reversibility of the band intensity upon delithiation. Note however that **(i)** the band at the lower Raman shift (552 and 602 cm^{-1}) show larger intensity as compared to LP40 while the one at higher wavenumber (1100-1500 cm^{-1}) have lower intensity, **(ii)** that overall, the signal fluctuation observed in the LP40 electrolyte is also observed in the LP57 and LP10 electrolytes, with however a lesser intensity.

Funded by the European Union
OPINCHARGE

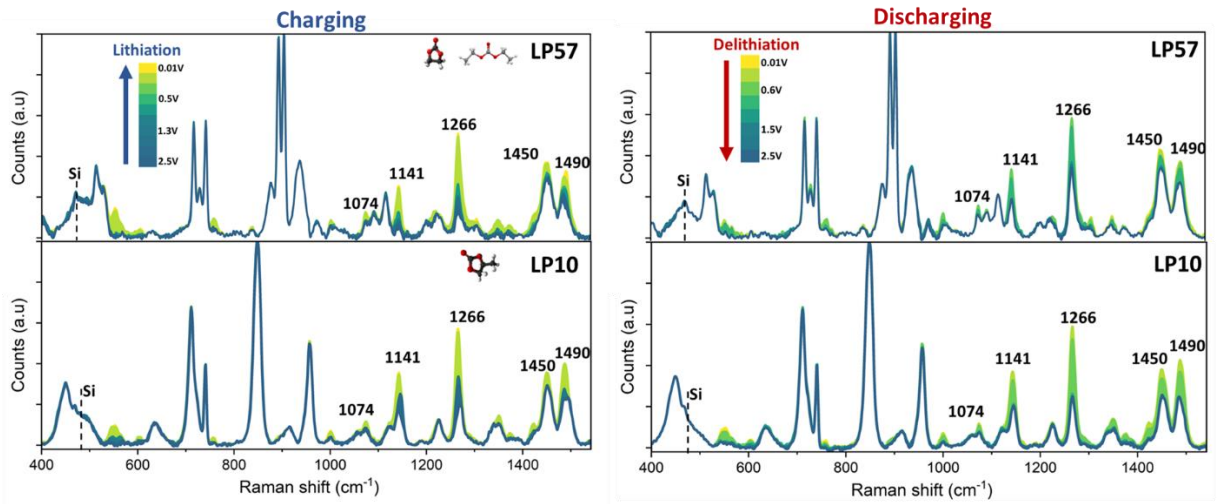

Figure 6: Operando SHINERS on doped Si (1st charge/discharge) in various electrolyte composition *- Potential dependent Raman response upon charging (**left**) and discharging (**right**) in LP57 electrolyte (**Top**), in LP10 electrolyte (**bottom**).*

The comparison of the band intensities at the end of the successive discharges, reveals a progressive build-up of signal intensity, cycle after cycle, associated to SEI product accumulation. LP40 showed the most pronounced accumulation, while LP10 showed the least. Surprisingly, in situ SHINERS measurements performed after 15 cycles reveal the opposite trend (lower SHINERS intensity in LP40), that could originate from a restructuring of the SEI at extended cycling. SEM images acquired after 15 cycles revealed that the SEI formed in the LP40 electrolyte exhibited a rougher morphology compared to those observed in LP57 and LP10. **This suggests a thicker but more heterogeneous (patchy) SEI formation in LP40 originating from a stronger instability and restructuring upon cycling**. The lower SHINER intensity in LP40 could originate from possible signal screening by the thick SEI built on the top of the SHINs but most likely as SHINs are still visible on SEM images by the strong variation of thickness across the different area where SHINER measurements were collected.

Funded by the European Union

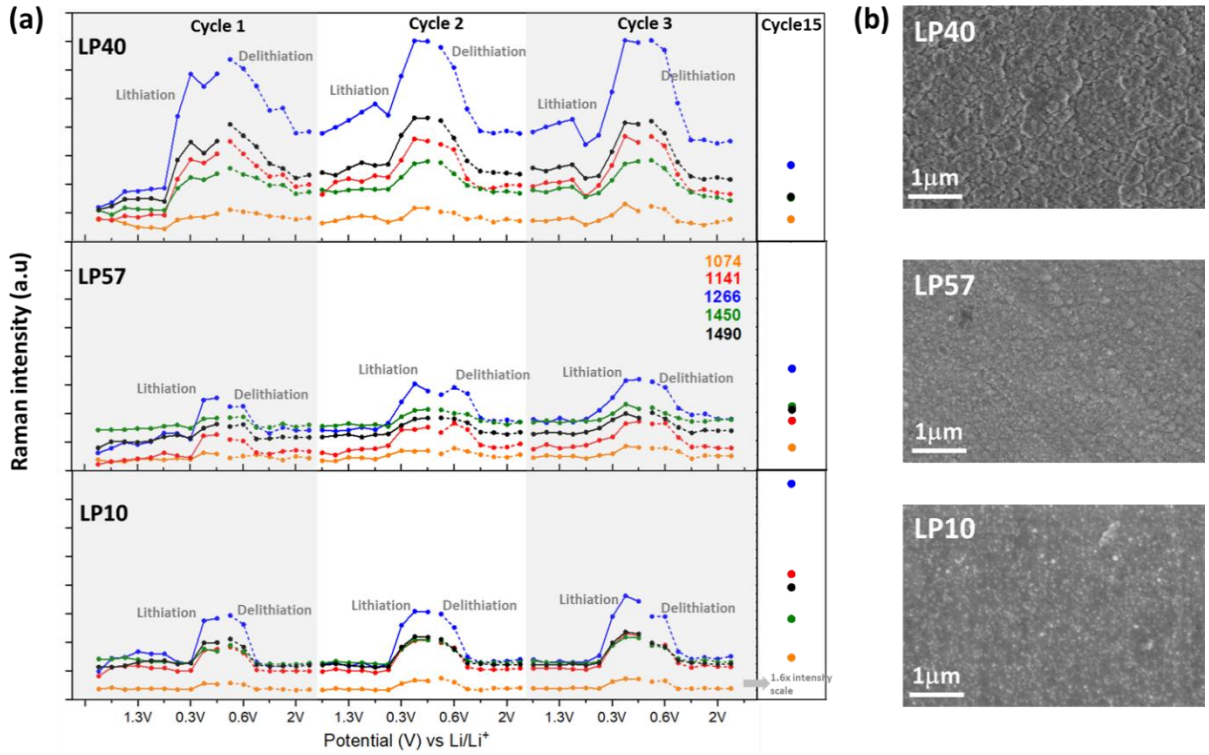

***Figure 7**: **Band intensity buildup at the end of the successive discharges of doped Si** - **(a)** Intensity fluctuations of selected Raman bands in different electrolytes over three cycles and at cycle 15, and **(b)** SEM image of the electrode after 15 cycles.*

Reference

(1) Schmitz, R.; Ansgar Müller, R.; Wilhelm Schmitz, R.; Schreiner, C.; Kunze, M.; Lex-Balducci, A.; Passerini, S.; Winter, M. SEI Investigations on Copper Electrodes after Lithium Plating with Raman Spectroscopy and Mass Spectrometry. *Journal of Power Sources* **2013**, *233*, 110–114. https://doi.org/10.1016/j.jpowsour.2013.01.105.

(2) Gu, Y.; You, E.-M.; Lin, J.-D.; Wang, J.-H.; Luo, S.-H.; Zhou, R.-Y.; Zhang, C.-J.; Yao, J.-L.; Li, H.-Y.; Li, G.; Wang, W.-W.; Qiao, Y.; Yan, J.-W.; Wu, D.-Y.; Liu, G.-K.; Zhang, L.; Li, J.-F.; Xu, R.; Tian, Z.-Q.; Cui, Y.; Mao, B.-W. Resolving Nanostructure and Chemistry of Solid-Electrolyte Interphase on Lithium Anodes by Depth-Sensitive Plasmon-Enhanced Raman Spectroscopy. *Nat Commun* **2023**, *14* (1), 3536. https://doi.org/10.1038/s41467-023-39192-z.

2. Assessment/quantification of side-reaction intensity - Identification of compositions (electrode/electrolyte) promoting the oxidative dissolution of cathode materials

Highlights

Funded by the European Union

OPINCHARGE

Results	Electrochemical crosstalk sensing technique with detection threshold for transition metal TM around 2.7 microM (higher than operando XAS or EPR) and with quantification accuracy (70%)
	Detection and capture of redox-shuttles upon short term cycling of LNMO/Li: transition metal (TM) Ni, Mn but also electrolyte oxydation products (< 8%)
	Capture of the distinct electrochemical signature of TM Ni and Mn (using µelectrode) and evidence of possible sensor selectivity by adjusting its polarization – The relative Ni/Mn detected amount does not scale directly with the stoichiometry in $LiNi_{0.5}M_{1.5}O_4$
	Stronger dissolution rate and extent of TM in LNMO in contact with electrolytes with lower resistance to oxidation (LP 40 vs LP57)
	Capture of crosstalk processes on NMC811 on longer term cycling & upon abusive polarization only. No evidence on LFP and LMFP on short-term cycling.
	Proof of concept of crosstalk sensing on full cell (LNMO/graphite) on the first charge/discharge
Outcomes	Publication: Dynamics of transition metal dissolution and cross-contamination in operating Lithium-ion batteries", Journal of Power Sources, 630, 2025, 236031 - https://doi.org/10.1016/j.jpowsour.2024.236031
	12 months project extension (Nantes Region funding) + internal IMN collaboration

2.1 Approach and implementation

Electrochemical sensor - Our new approach for operando crosstalk sensing introduces within the electrode assembly, a polarized platinum mesh (sensor) so that redox active oxidation products generated at the positive electrode upon charging (and diffusing/migrating toward the negative electrode, i.e. redox shuttles) can be reduced and potentially trapped by electroplating, while avoiding electrolyte reduction. This real-time crosstalk sensing technique (supported by possible ex situ chemical analysis of the sensor) allows dynamic quantification of the extent of metal dissolution from the positive electrode at each operating voltage of the electrode material.

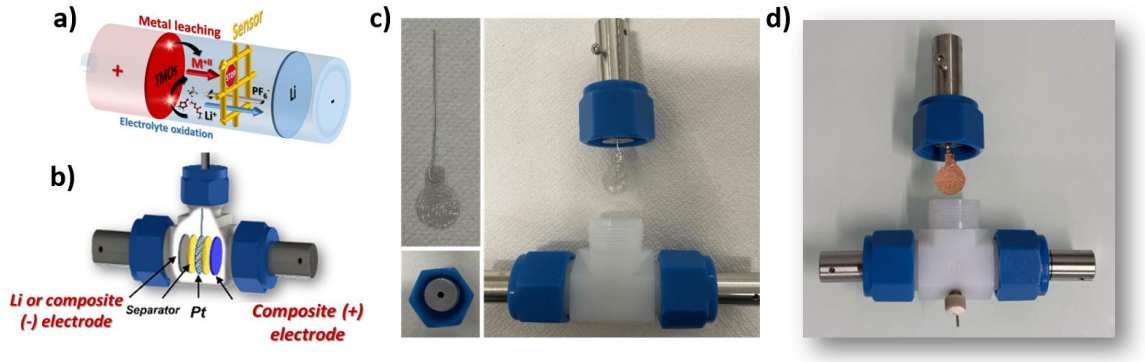

Figure 8 Crosstalk sensing device - (a) *Concept,* ***(b)*** *electrode assembly,* ***(c)*** *3-electrode T-shape Swagelok cell,* ***(d)*** *4-electrode T-shape Swagelok cell*

Implementation - The metallic sensor is intercalated between the positive and negative electrode (Li metal or graphite) and electrically insulated using separator in a T-shape Swagelok cell: (+)

Funded by the European Union

composite electrode|Ptsensor|Li (-). The positive composite electrode is charged/discharged at a given C-rate (C/10, C) while the sensor is maintained at a constant polarization (constant voltage measured vs lithium). The calibration of the sensor (capture efficiency, time response and detection threshold) has been achieved previously on a copper/lithium system, polarized to produced known amounts of dissolved copper in the electrolyte (Technical report M1-M18 and final report).

Several crosstalk sensing configurations have been tested:

- **Various metallic sensors** have been tested circular Pt mesh (2 different mesh size) and foam electrode (Ni and Cu) - *High surface sensor do not show higher capture efficiency but a higher background current impacting the sensitivity and also quantification accuracy.*
- **Various separators** have been evaluated: thick glass fiber (Whatman GF/D) or thin polyolefin membranes (Celgard). *Same capture efficiency was found with both separators, with however a more detailed response with Celgard (less convoluted by transport mechanism)*
- **Various polarisation schemes** of the sensor for selective metal trapping have been tested
- **Various cell set-ups,** a first 3-electrode sensing setup has been since upgraded to a 4-electrode set-up, using an additional Li-electrode used either as reference or counter electrode.

2.2 Operando crosstalk sensing on battery materials

2.2.1 LNMO positive electrode materials (half-cell vs full-cell)

The operando crosstalk sensing technique was first developed, tested and optimized on half-cells of LNMO/Li, then a 4-electrode cell was developed (additional ref electrode) to track and control the true potential of the sensor, LNMO and counter electrodes (Li or graphite) upon cycling.

2.2.1.1 Half-cell LNMO / Li

Impact of electrolyte composition **-** A proof of concept of crosstalk sensing on LNMO/Li was published in 2025, showing reduction current at the Pt sensor polarized at 1V upon LNMO cycling in LP57, the intensity of which fluctuates with time, indicating the **various dissolution rate and extent depending on the stage of operation of LNMO**. **Metal leaching** seems to take place at all stages of operation upon **charging but also discharging**. The post-mortem analysis of the sensor by SEM-EDX and XRF confirmed after 5 cycles (C/10) the presence of metal deposits (+ electrolyte residues) on the mesh sensor with mostly Mn detected. Further analysis (dQ/dV curves) revealed a more pronounced dissolution around $Ni^{+II/+III}$ & $Ni^{+III/+IV}$ operation voltage as compared to $Mn^{+III/+IV}$. By changing the electrolyte to LP40, with lower resistance to oxydation than LP57, much higher charge were detected on the sensor (170 vs 100 µAh after 5 cycles), confirming that electrolyte degradation at high potential promotes the dissolution mechanism of TMOs.

Funded by the European Union

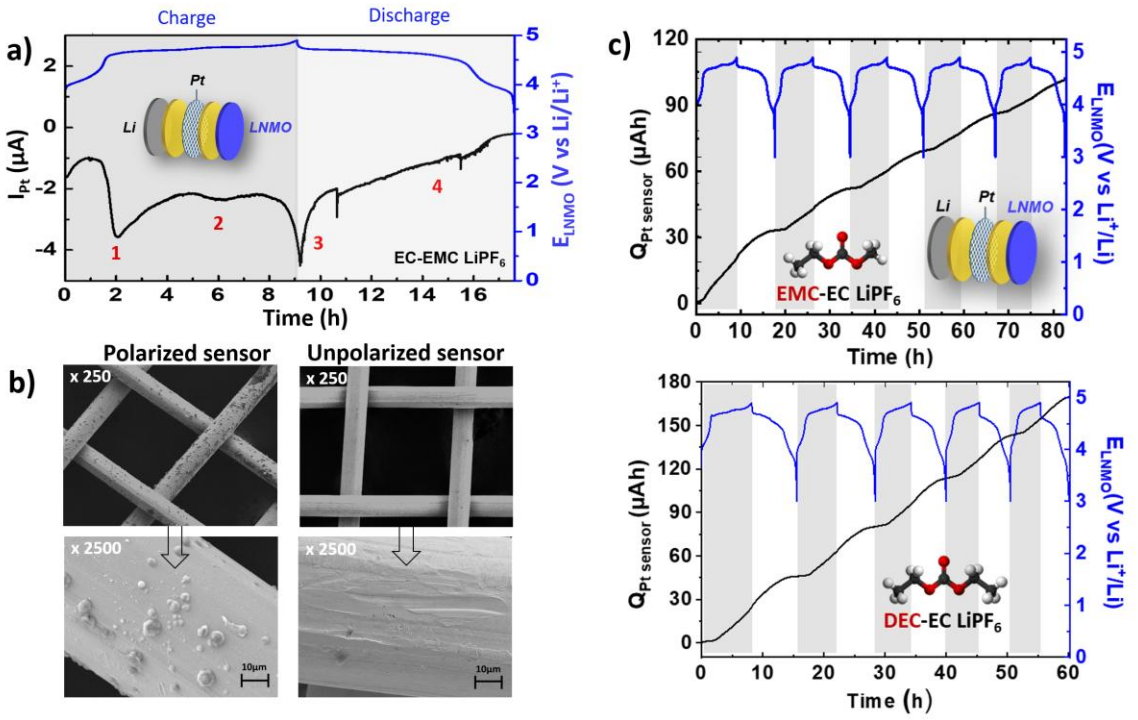

Figure **9**: ***Crosstalk sensing on the operating LNMO/Li system & impact of the electrolyte composition*** - ***(a)*** *Potential profile of LNMO upon charging and discharging at C/10 in LP57 electrolyte (first cycle, in blue) and reduction current measured at the platinum grid sensor biased at 1 V vs Li/Li⁺ (chronoamperometry, in black),* ***(b)*** *SEM post-mortem analysis of the biased platinum mesh evidencing surface deposits as compared to the non-polarized (OCV) mesh,* ***(c)*** *Crosstalk sensing experiments carried out in 2 different electrolytes LP57 (top) vs LP40 (bottom). The accumulated charge at the sensor is plotted together with the potential profiles of LNMO upon charging and discharging at C/1 (5 cycles).*

Sensor selectivity - To assess the crosstalk sensing selectivity, i.e. the selective detection of Ni and Mn for LNMO, the Pt sensor mesh was replaced by a Pt microelectrode, delivering a background free electrochemical response. Constant CV cycling of the Pt µ electrode was implemented during the first charge of LNMO/Li, revealing distinct EC signature depending on the operation stage of LNMO. When polarizing from the OCV to the first $Mn^{+III/+IV}$ stage, two main current peaks (potential onset at around 2.8 and 2V) appear then progressively diminish. Similar behavior is observed during the $Ni^{+II/+III}$ stage and then the sensor shows almost no variation during the $Ni^{+III/+IV}$ stage. The decrease and decrease of may correspond to the fluctuating Ni and Mn leaching rate depending on the LNMO operation stage and to their constant extraction from the electrolyte by their reduction at the Li CE. For the $Ni^{+III/+IV}$ stage, with possible lesser dissolution rate, the sensor detection limit may be reached.

Then, crosstalk sensing experiments were conducted on Pt mesh sensor at different polarization to selectively capture Ni only (at E_{Sensor} = 2V) and Ni & Mn together (at E_{Sensor} = 1.3V). The current profile measured at 1.3 and 2V show the same fluctuations with time, meaning that the same processes (dissolution mechanism at a given potential) is probably captured but with a lesser intensity. The accumulated charge at 1.3 is higher than that at 2V, i.e. 21.5 vs 13.7 µA at the end of the first cycle, as expected since both Mn et Ni are expected to be captured at 1.3V. The detected amount of leached metal at 1.3V & 2V does not scaled directly with LNMO stoichiometry ($LiNi^{+II}0.5Mn^{+IV}1.5O_4$), as 4-time more metal could be expected to be detected at 1.3V than at 2V if all metal centres in LNMO were to be dissolved. Further investigation of the sensor polarization effect coupled to post-mortem characterization by XRF are needed to deepen our understanding of the sensor selectivity.

Funded by the European Union
OPINCHARGE

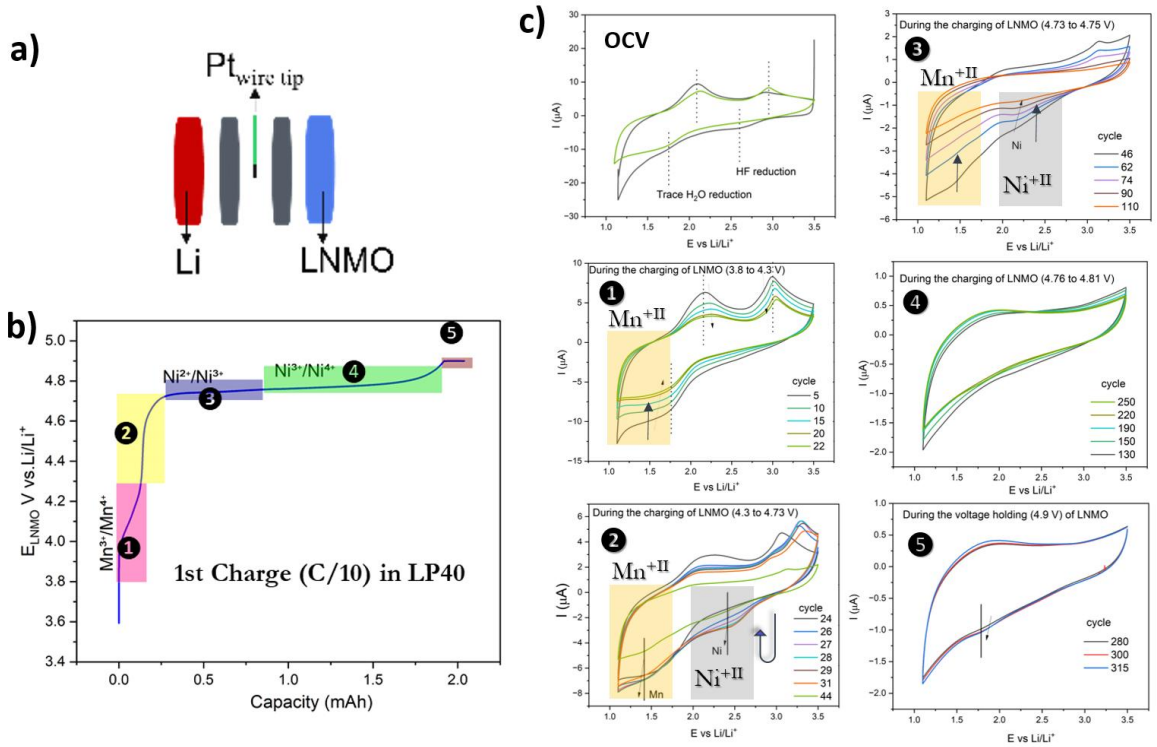

Figure 10 Electrochemical signature of redox shuttles - (a) *Concept: sensor mesh replaced by a Pt µelectrode,* ***(b)*** *LNMO voltage profile (cycling at C/10 in LP40),* ***(c)*** *CV response of the Pt µsensor at different stage of operation of LNMO (see correspondance on (b).*

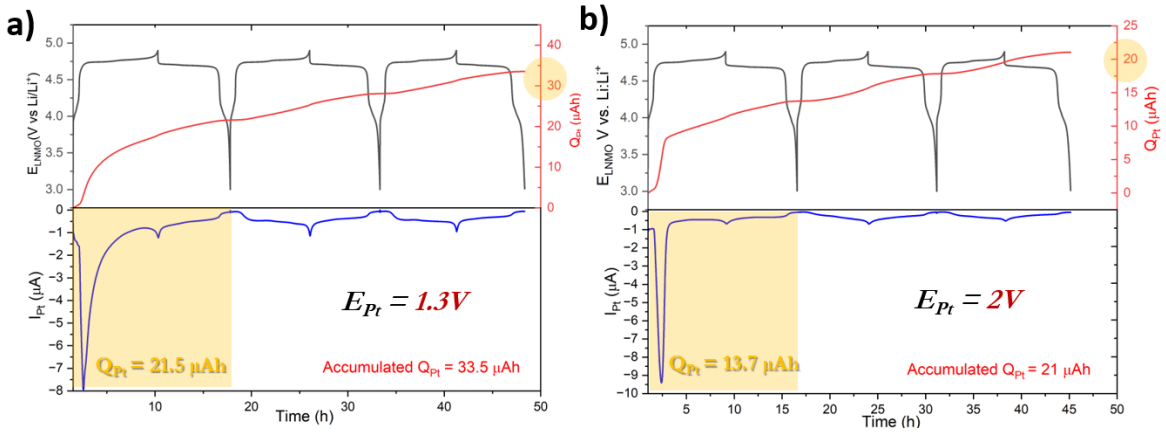

Figure 11 Selective crosstalk quantification *– Crosstalk sensing experiments on LNMO/Li cycled at C/10 in LP40 electrolyte with the sensor Pt mesh polarized at* ***(a)*** *1.3V and* ***(b)*** *2V. Top: LNMO voltage profile (black) and charge accumulated at the Pt sensor, bottom: current measured at the sensor.*

2.2.1.2 Full-cell LNMO / graphite

Preliminary crosstalk sensing tests were conducted on LNMO/graphite full cell, for which the potential of both electrodes fluctuates with the state of charge (SOC). To control precisely the polarization of the sensor, when lithium CE (almost fixed potential) is replaced by a graphite composite anode, a 4-electrode cell was design, incorporating a reference lithium electrode positioned to the side of the electrode assembly. The sensor response during the first charge is equivalent to the one observed in half-cell, meaning that possible degradation products generated at low potential on graphite do not interfere with the crosstalk sensing (or in a similar way as with Li). However, by the end of the first discharge, a strong reduction current is detected on the sensor, the intensity of which increases considerably cycle after cycle. Leaching of copper soluble species from the current collector

Funded by the European Union
OPINCHARGE

of graphite can explain the observed behavior. As the metal senor draws electrons from the graphite during both charge and discharge, the potential of graphite rises at the end of the discharge (when all lithium ions have been extracted) to supply the current (even small) at the grid, and reaches the oxidative potential of copper. To circumvent this problem, the side lithium will be used in future experiments as counter/reference electrode for the mesh sensor, avoiding possible interference with the cycling of LNMO/graphite.

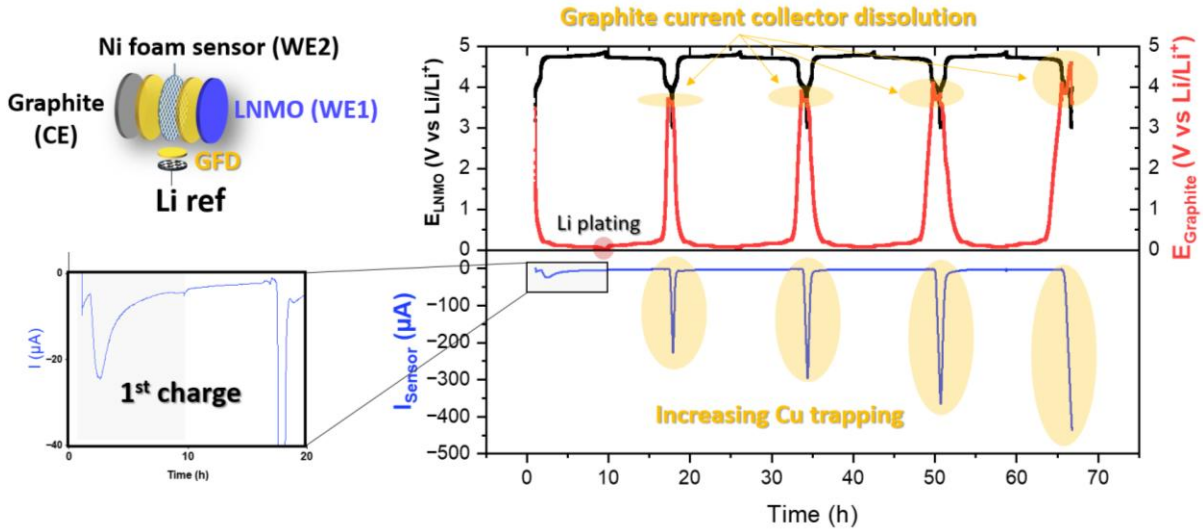

*Figure **12** Crosstalk sensing on full cell (LNMO/graphite) – Top left: 4-electrode cell configuration, Top right: Potential response of both LNMO and graphite electrode upon cycling (C/10 in LP57 electrolyte), Bottom right: sensor response (polarization at 1.3V), Bottom left: zoom on the sensor response during the first charge.*

2.2.2 Other positive electrode materials

Other Tests on material with lower dissolution rates (as compared to LNMO), such as LMFP, LFP, demonstrated low signal to noise ratio using a 3-electrode cell, affecting the detection of crosstalk processes. The NMC811 positive electrode material, which was not in the list of suggested materials in the project, has been added and provided by our partner (Cidetec). NMC811 is known to be much more stable that LNMO and crosstalk phenomena if they occur are much less pronounced on the short-term cycling. As a matter of fact, a detectable response of the sensor was only observed on longer cycling and under abusive polarization conditions of NMC811 (> 4.9V). The post-mortem analysis of the sensor confirms the presence of Ni, Mn and Co deposits.

Funded by the European Union

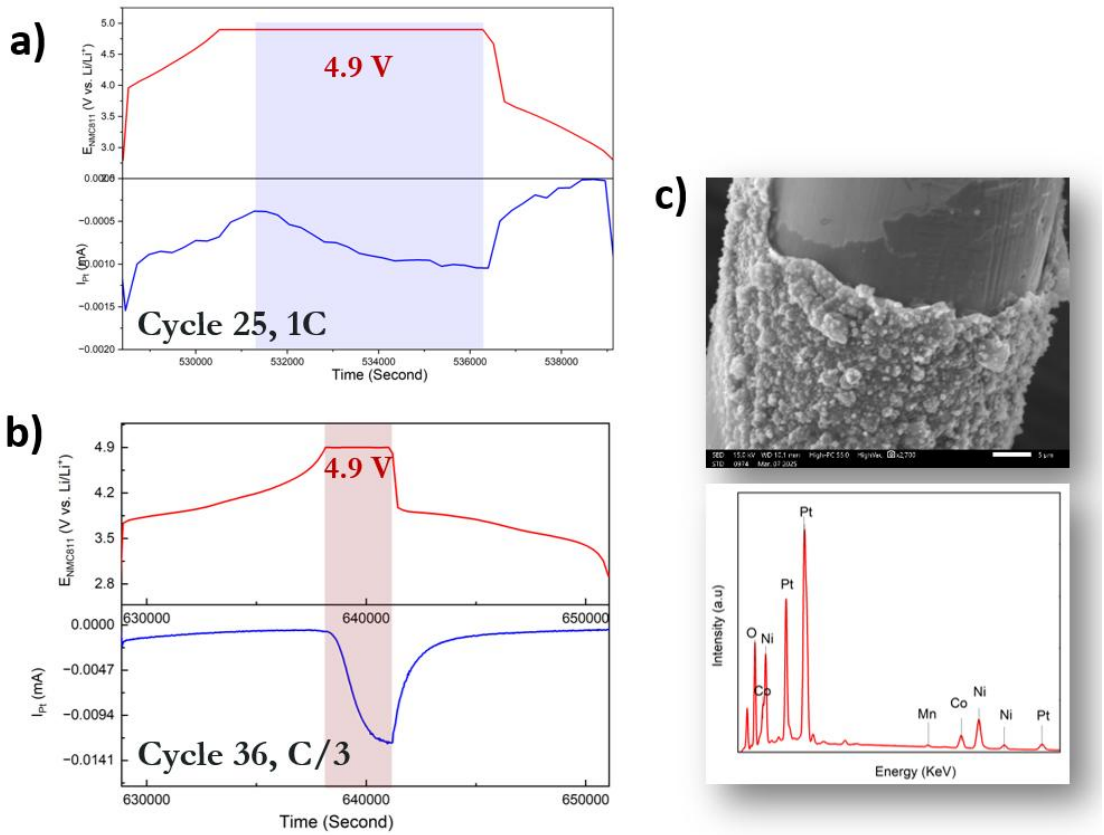

Figure14 Crosstalk sensing on the operating NMC811/Li system *- NMC811 voltage profile upon cycling (abusive cutoff voltage at 4.9V) and concomitant sensor response:* ***(a)*** *at cycle 25 (1C),* ***(b)*** *at cycle 36 (C/3),* ***(c)*** *post-mortem SEM-EDX analyses.*

Funded by the European Union